J. Appl. Cryst. (1992). **25**, 366–371

Simulation of Renninger Scans for Heteroepitaxic Layers

By C. A. B. Salles da Costa and L. P. Cardoso

Instituto de Física-UNICAMP, CP 6165-13081, *Campinas, SP, Brazil*

and V. L. Mazzocchi and C. B. R. Parente

IPEN-CNEN/SP, CP 11049-*Pinheiros* 05499, *São Paulo, SP, Brazil*

(*Received* 21 *May* 1991; *accepted* 16 *January* 1992)

Abstract

In this work, X-ray Renninger scans for semiconductor single-crystal and heteroepitaxic structures are simulated. The simulation program is based on the iterative method for the calculation of multiple diffraction in imperfect crystals. The calculated diffracted-beam path length takes into account the small thickness of the heteroepitaxic layers in order to reproduce the survival of only surface secondary reflections in the layer Renninger scans. Applications of these simulations for bulk material (GaAs, GaSb), binary layers (GaAs/Si) and ternary layers (InGaAs/GaAs) show very good agreement with the corresponding experimental scans.

Introduction

The possibility of providing three-dimensional information about the crystalline lattice and its sensitivity to small lattice deformations (symmetry changes) make X-ray multiple diffraction, as reported by Chang (1984), a very useful technique for studying epilayered materials.

The multiple diffraction of the sample is systematically measured in the Renninger geometry. The sample is adjusted to set a primary crystallographic plane (h_P, k_P, l_P) whose normal is parallel to the rotation axis, φ, keeping the scattering vector in the diffraction condition while the sample is rotated around this axis. During rotation, the incident beam can be scattered by other, secondary, planes (h_S, k_S, l_S) asymmetrically with respect to the crystal surface. Then, in the continuous background representing the primary intensity, *Umweganregung* peaks and/or *Aufhellung* dips will appear corresponding to the interaction between the primary and the several secondary reflections. Upon multiple diffraction, this interaction occurs through the coupling planes $[(h_P - h_S), (k_P - k_S), (l_P - l_S)]$, which transfer intensity from the primary to the secondary beam or *vice versa*. Thus, the Renninger scan (RS) is the representation of these interactions observed through the primary-intensity oscillations. In fact, peaks can only be seen when a space-group-forbidden primary reflection is chosen.

Soejima, Okazaki & Matsumoto (1985) and Rossmanith (1986) have published RS simulation programs that are based on X-ray kinematical theory. The effect of higher-order diffraction (n-beam interaction, $n > 3$) is treated in both as the sum over the secondary reflections of the $(n - 2)$ pairs of three-beam cases. Rossmanith, Kumpat & Schulz (1989) have developed the program designed by Rossmanith, making it faster and implementable on a PC. More recently, Salles da Costa, Cardoso, Mazzocchi & Parente (1990) have described a program (*MULTX*) to simulate RS for X-rays. In *MULTX*, the theoretical integrated intensities are calculated step by step using the iterative method for the multiple-diffraction calculation for imperfect crystals reported by Parente & Caticha-Ellis (1974). It uses the general term of the Taylor series and allows for many-beam interactions to be simultaneously considered. Since a large number of terms is easily calculated by the computer, the *MULTX* program can be used in cases of high absorption and/or high secondary extinction.

It should be noted that the path lengths of the several beams involved in multiple-diffraction phenomena play a very important role in intensity calculations. This justifies our effort in developing the calculations of the path lengths.

In this work, the diffracted-beam path-length calculation was improved so that the RS for binary and ternary heteroepitaxic structures could be simulated and compared with the experimental ones. Interesting multiple-diffraction features, such as the drastic decrease in the intensity for Bragg and Laue secondary reflections are expected to appear in both RS.

The diffracted-beam path lengths

Of the multiple-diffraction phenomena, the surface secondary reflections constitute a special case,

0021-8898/92/030366-06$06.00

since they are diffracted parallel to the primary atomic planes. Generally, these primary planes are parallel to the sample surface. The geometrical representation of these beams on the Ewald sphere is shown in Fig. 1. One can observe that all surface reflections lie on the equatorial plane. In case of heteroepitaxic structure analysis, once the layer thickness is reduced, the surface reflections must play the most important role in the layer RS. For a 002 primary reflection in a zinc blende structure, all secondary reflections with Miller indices $(h, k, 1)$ correspond to surface reflections. In fact, the layer thickness reduction is not too important for these special reflections. However, it strongly affects the Bragg or Laue secondary reflections, which depend on the diffracting material volume. Here, we describe a new method for taking into account the diffracted-beam path lengths in the calculations, which is rather different from the geometrical approach previously reported (Salles da Costa, Cardoso, Mazzocchi & Parente, 1990).

The average path length of the different diffracted beams at depth x below the surface of a plane parallel plate of thickness T, including the incident-beam distance, is given by Caticha-Ellis (1969) as

$$\langle x/\gamma\rangle = 1/\mu - (T/\gamma)[\exp(-\mu T/\gamma)]/[1-\exp(-\mu T/\gamma)]. \quad (1)$$

Here μ is the linear absorption coefficient. Furthermore,

$$\langle x/\gamma\rangle = \langle x\rangle/\gamma_0 + \langle x\rangle/\gamma_i = l_0 + l_i, \quad (2)$$

where l_0 and l_i are the incident- and diffracted-beam path lengths and $1/\gamma = 1/\gamma_0 + 1/\gamma_i$; γ_0 and γ_i are the direction cosines for the incident and the diffracted beams with respect to the normal to the plate surface, respectively.

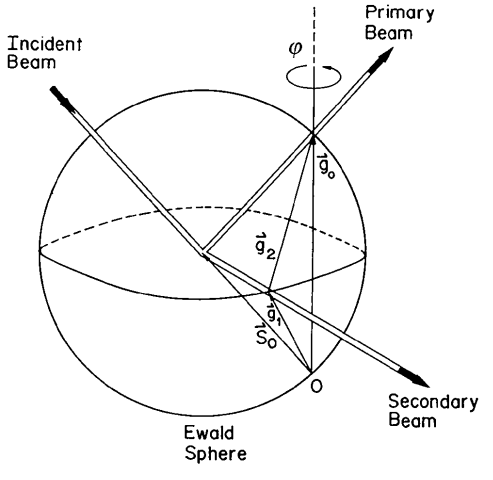

Fig. 1. Representation of a surface three-beam case in the reciprocal space. The vectors $\mathbf{g}_0$, $\mathbf{g}_1$ and $\mathbf{g}_2$ are the normals to the primary, secondary and coupling planes, respectively.

By considering a highly absorbing crystal

$$\langle x/\gamma\rangle = 1/\mu, \quad (3)$$

one can obtain

$$l_0 = \langle x\rangle/\gamma_0 = (1/\mu)(\gamma/\gamma_0)$$

and

$$l_i = \langle x\rangle/\gamma_i = (1/\mu)(\gamma/\gamma_i).$$

Moreover, if the primary reflection is symmetric, $\gamma_0 = \gamma_1$, $\gamma/\gamma_0 = \gamma/\gamma_i = 1/2$ and $l_0 = l_1 = 1/2\mu$ which gives

$$l_i = \langle x\rangle/\gamma - l_0 = 1/\mu - 1/2\mu = 1/2\mu \quad (4)$$

for all secondary reflections.

However, in the layer case where the thickness is too small, (4) is no longer valid for all Laue or Bragg secondary reflections. We use instead (2) in the form

$$l_0 = \langle x/y\rangle - l_i \quad (5)$$

where $\langle x/y\rangle$ is given by (1).

By using the above conditions for a primary symmetric reflection and taking $l_i = l_1$, (5) can be written as

$$l_0 = 1/2\mu - (T/\gamma_0)[\exp(-2\mu T/\gamma_0)] \times [1-\exp(-2\mu T/\gamma_0)]^{-1}. \quad (6)$$

Then, the average path length is

$$l_i = 1/2\mu - (T/\gamma)[\exp(-\mu T/\gamma)]/[1-\exp(-\mu T/\gamma)] + (T/\gamma_0)[\exp(-2\mu T/\gamma_0)]/[1-\exp(-2\mu T/\gamma_0)] \quad (7)$$

As for the surface secondary reflections in the layer case, for a highly absorbing crystal ($\mu T \simeq 10^{-3}$), we have

$$\langle x/\gamma\rangle = 1/\mu. \quad (8)$$

Therefore, the average path length of the surface diffracted beam is

$$l_s = 1/\mu - l_0 = 1/2\mu + (T/\gamma_0)[\exp(-2\mu T/\gamma_0)] \times [1-\exp(-2\mu T/\gamma_0)]^{-1}. \quad (9)$$

In the high-thickness limit, (6) and (7) assume the value $1/2\mu$ which is the same already obtained in the bulk case, as expected. In turn, in the low-thickness limit (layer range) one can observe that l_s is at least one order of magnitude greater than l_i. This fact has a remarkable effect on the layer RS since only the surface secondary reflections contribute to this scan, although weak peaks corresponding to the strongest Bragg or Laue reflections can also be detected.

Experimental

The RS measurements were carried out on a geometrical arrangement which consists of: an X-ray

Table 1. *Diffracted-beam path lengths l* (cm) *involved in the* 002 GaAs *Renninger scan for layers of different thicknesses, calculated by the MULTX program.*

The path lengths for the primary, surface and Laue–Bragg reflections are shown together with the layer lattice parameter used in their calculation.

hkl	$a = 5.6614$ Å, $c = 5.6481$ Å, $t = 1.0$ μm	$a = 5.6593$ Å, $c = 5.6463$ Å, $t = 2.0$ μm	$a = 5.6629$ Å, $c = 5.6457$ Å, $t = 4.2$ μm	$a = 5.6619$ Å, $c = 5.6450$ Å, $t = 5.0$ μm	Bulk $a = 5.6534$ Å, $t = 350$ μm
002	0.000174	0.000331	0.000615	0.000699	0.001241
311	0.002313	0.002154	0.001873	0.001788	0.001241
$\bar{1}\bar{1}1$	0.002313	0.002154	0.001873	0.001788	0.001241
$(\bar{1}3\bar{1})(\bar{1}\bar{3}3)$	0.000091	0.000179	0.000364	0.000428	0.001241
$\bar{1}5\bar{1}$	0.002313	0.002154	0.001873	0.001788	0.001241
$5\bar{5}1$	0.002313	0.002154	0.001873	0.001788	0.001241
$(5\bar{3}\bar{1})(5\bar{3}\bar{3})$	0.000091	0.000179	0.000364	0.000428	0.001241
$5\bar{1}\bar{1}$	0.002313	0.002154	0.001873	0.001788	0.001241

divergent-beam source (Cu $K\alpha$) with an effective focal size of 50 × 50 μm; a collimator of length 330 mm, positioned between the crystal and the X-ray window, which provides an incident beam of 3′ divergence; a horizontal goniometer with Eulerian cradle to provide automatic RS (φ axis with stepping motor); and a scintillation detector with its associated electronics.

As for the samples, the GaAs and GaSb bulk materials are pieces of commercial wafers of thickness 350 μm. The GaAs layer (1 μm) was grown by vacuum chemical epitaxy (VCE) on top of a [001] Si substrate (Barreto, Carvalho, Ito & Fraas, 1987), whereas the ternary layer InGaAs (0.2 μm) was grown by metallorganic chemical vapour deposition (MOCVD) on top of a [001] GaAs substrate (Sacilotti & Bordeaux Rego, 1989).

Results and discussion

The 002 GaAs weak reflection was used as the primary reflection. The intensities in each simulation were approximately normalized to the strongest experimental intensity, possible variations due to the adjusted value for the plotter scale being small.

Table 1 shows the diffracted-beam path lengths corresponding to different reflections calculated using the program *MULTX* for several layer thicknesses. In the calculations, the lattice parameters used for the GaAs layers were those quoted by Lum *et al.* (1988), which are indicated for each thickness value. For comparison, the path length calculated in the GaAs bulk case as $l = 1/2\mu$ for all secondary reflections is also shown. One can observe in Table 1 that there are only three different l values corresponding respectively to the 002 primary reflection, to all possible ($l = 1$) surface secondary reflections represented by 311, $\bar{1}\bar{1}1$, $\bar{1}5\bar{1}$, $5\bar{5}1$ and $5\bar{1}\bar{1}$ and the four-beam Laue–Bragg cases, involving the ($l = -1$ and 3) reflections represented by $\bar{1}3\bar{1}$ $\bar{1}\bar{3}3$ and $5\bar{3}\bar{1}$ $5\bar{3}\bar{3}$. It is very important to notice the large variation of l_i with respect to l_s: both present the same value in the bulk case, but l_i is equal to $l_s/25$ in the 1 μm layer case. The average is taken by considering the path-length values at depth x: that is, when the layer thickness decreases, the average value is approximately equal to the surface path length, which is the greatest value in the averaged region (since l includes the incident-beam distance). In the three-beam surface case, the secondary planes diffract the incident beam directly towards the primary direction, giving rise to the visible surface peaks in the layer RS. Therefore, for thinner layers, the observed surface-peak intensities are strong, from the multiple-diffraction viewpoint, because the secondary surface-beam intensity is transferred to the primary. This is in contrast with the kinematical point of view, which indicates complete absorption of these beams as the surface path lengths are the largest.

The influence of the layer thickness on the RS is shown in Fig. 2 through the several simulated scans for the interval $96 \leq \varphi \leq 126°$. For this we have also used a GaAs layer of thickness 350 μm, which is similar to the bulk material illustrated in Fig. 3. The lattice parameters and layer thicknesses used in the simulations are those listed in Table 1. Although the intensity scales are in arbitrary units, the same scale has been used for all scans. The analysis of the intensity of the $(\bar{1}3\bar{1})$ $(\bar{1}\bar{3}3)$ Laue–Bragg peak shows the striking effect of the layer thickness, *i.e.* when the thickness increases, the peak intensity becomes stronger. On the other hand, for the $(\bar{1}5\bar{1})$ surface peak, a reverse effect occurs although to a lesser degree; the peak intensity becomes weaker with the increase in layer thickness. The other Laue–Bragg and surface peaks appearing in the RS provide analogous results when analysed.

By simple comparison between a Laue–Bragg peak and a surface peak in Fig. 2, the scans corresponding to different thicknesses can be clearly discriminated. This result shows the strong effect of the diffracted-beam path lengths on the intensities in a RS.

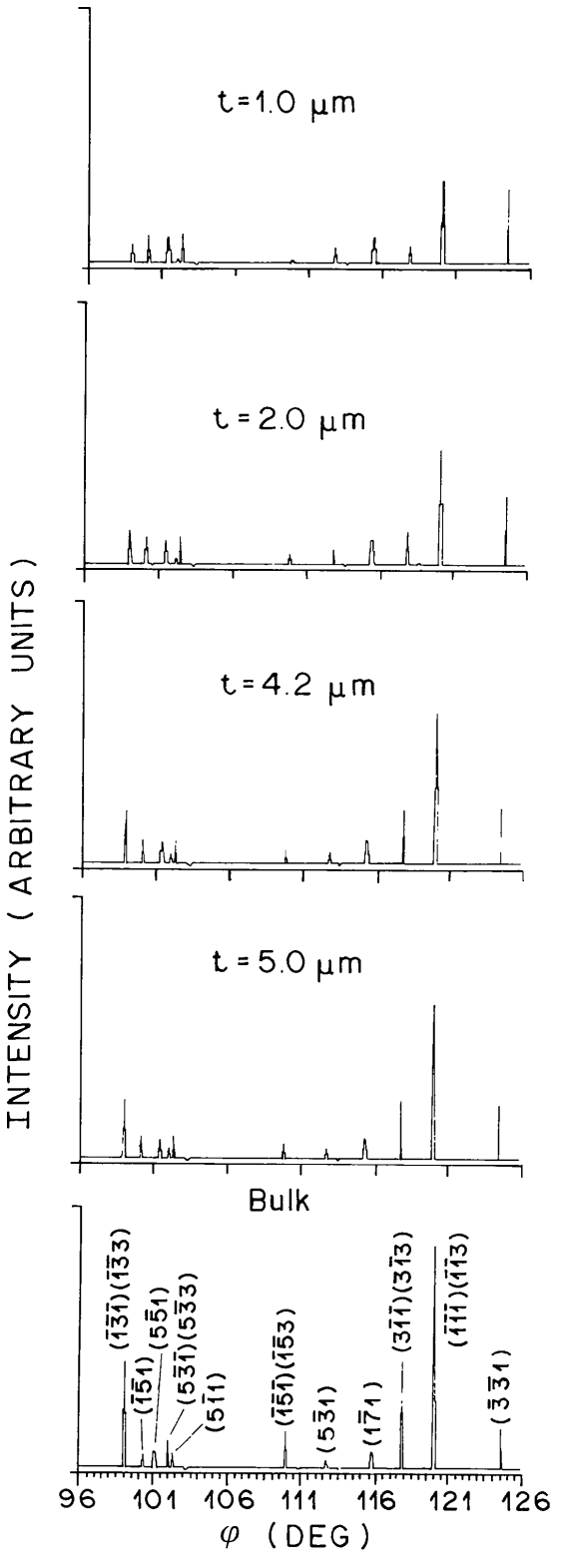

Fig. 2. Simulated 002 GaAs Renninger scans using Cu $K\alpha_1$ for different layer thicknesses to show the influence of the diffracted-beam path lengths on the intensities in a RS. Bulk thickness: 350 μm.

Fig. 3 shows the RS for GaAs bulk material. The experimental scan in Fig. 3(*a*) is compared with the simulated one in Fig. 3(*b*) to illustrate the good agreement obtained. In the calculations, we used a lattice parameter $a = 5.6535$ Å, a step size of $\Delta\varphi = 0.045°$, isotropic thermal parameters $B_{Ga} = B_{As} = 0.6$ Å^2 and a mosaic spread $\eta = 0.05°$ (9×10^{-4} rad). Although 30 terms in the expansion were considered, the series converged after 6 terms. The value $1/2\mu$ was used as the diffracted-beam path length for all secondary reflections. The peak positions in both theoretical and experimental RS are also in very good agreement. As a check of the simulation, the reliability factor (R) was calculated by using

$$R = \sum |I_{calc} - I_{exp}|/I_{exp}$$

where the summation is over all peaks in a specified range, I_{calc} stands for the theoretical maximum intensities of the peaks, corrected by the scale factor, and I_{exp} are the corresponding experimental intensities. In the case of Fig. 3, using all peaks detected in an interval $83 \leq \varphi \leq 104°$ in the RS, R turns out to be 0.09, which supports the validity of the treatment as well as the assumptions made in this work.

Fig. 4(*a*) shows a typical experimental RS for GaSb bulk material in which the 002 reflection is strong enough to emphasize the energy interaction between the primary and the secondary reflections giving rise to *Umweganregung* peaks and *Aufhellung* dips. The *MULTX* program is able to simulate both multiple-diffraction features as shown in Fig. 4(*b*). The

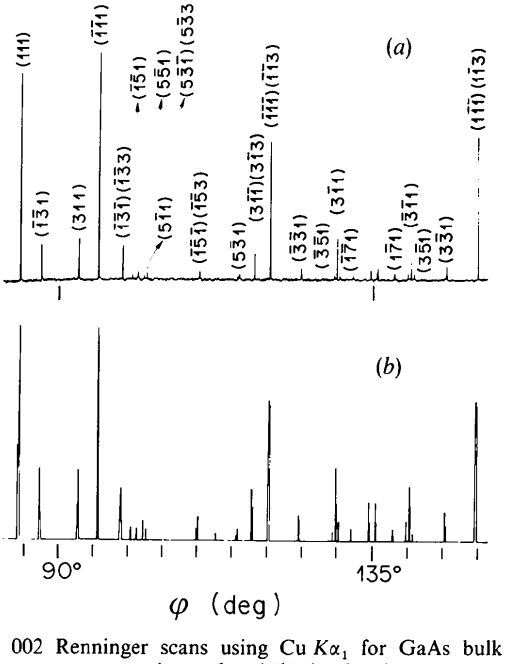

Fig. 3. 002 Renninger scans using Cu $K\alpha_1$ for GaAs bulk: (*a*) experimental and (*b*) simulated.

parameters $a = 6.095$ Å, $B_{Ga} = 0.66$ Å^2, $B_{Sb} = 0.60$ Å^2, $\Delta\varphi = 0.045°$ and $\eta = 9 \times 10^{-4}$ rad were used in the simulation. A good agreement is obtained from the comparison between the experimental and simulated scans.

An application of RS simulation to the heteroepitaxic structure GaAs/Si is depicted in Fig. 5. The experimental RS for a thin (1 μm) GaAs layer on top of an Si [001] substrate is shown in Fig. 5(*a*) together with the corresponding simulated RS of this layer in Fig. 5(*b*). The simulation is made for $a = 5.6614$, $c = 5.6481$ Å, $\Delta\varphi = 0.05°$, $B_{Ga} = B_{As} = 0.6$ Å^2, $\eta = 0.068°$ (1.2×10^{-3} rad). From the comparison of the first scan with that depicted in Fig. 3(*a*), one can clearly observe the striking effect of the reduction in the layer thickness on the RS. Whereas all surface secondary peaks are visible, the Bragg or Laue reflections practically disappear, except for the strongest 000 002 $\bar{1}\bar{1}1$ $1\bar{1}3$ four-beam case, which gives a weak contribution. The new method for the diffracted-beam path length presented here is able to simulate even this weak peak, as depicted in Fig. 5(*b*).

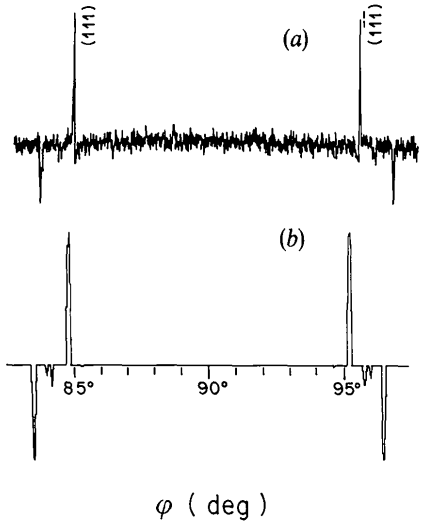

Fig. 4. Portion around $\varphi = 90°$ of the 002 GaSb Renninger scan using Cu $K\alpha_1$: (*a*) experimental and (*b*) simulated. The peak asymmetry indicative of the good quality of the crystal cannot be simulated, since the *MULTX* program only applies to mosaic crystals.

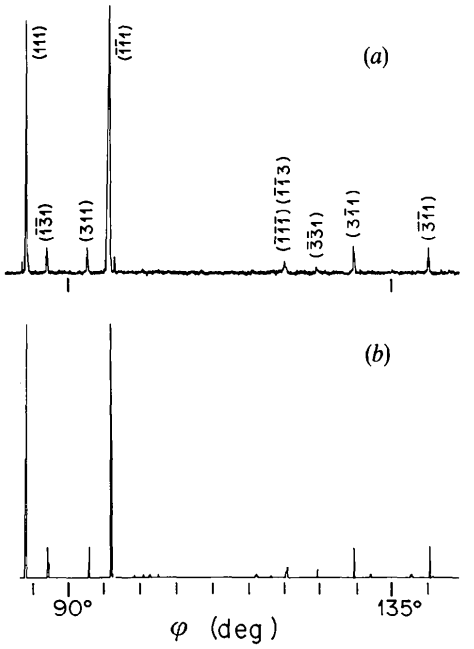

Fig. 5. 002 Renninger scans using Cu $K\alpha_1$ applied to heteroepitaxic structures. (*a*) Experimental RS for a GaAs layer on top of an Si substrate and (*b*) the corresponding simulated RS.

In Fig. 5(*a*), the effect of lattice strain for such a highly mismatched epitaxic layer as GaAs/Si can be seen through the broadening of the surface peaks. Moreover, the small extra peaks close to the 111 and $\bar{1}\bar{1}1$ peaks correspond to the first observation of hybrid multiple diffraction in a RS (Morelhão, Cardoso, Sasaki & Carvalho, 1991). These diffractions, due to the layer/substrate lattice interaction, occur when the beam first diffracted by a substrate (or layer) secondary plane crosses the interface between both materials to be rescattered by a layer (or substrate) coupling plane towards the detector. Hybrid multiple diffraction has been observed and described in X-ray divergent-beam experiments by Isherwood, Brown & Halliwell (1981) and simulated by Morelhão & Cardoso (1991). Therefore, only extra *Umweganregung* peaks can contribute as hybrid reflections to layer (or substrate) RS in previously determined positions. This hybrid multiple diffraction cannot be simulated by the *MULTX* program, as is observed in Fig. 5(*b*), since the program does not account for the layer/substrate interactions. However, the agreement for all remaining peaks is very good.

Since this paper deals with the simulation of heteroepitaxic-layer RS, it is interesting to present an application of the *MULTX* program to the $In_xGa_{1-x}As/GaAs$ structure. The experimental 002 RS for the ternary layer with $x = 0.035$ is shown in Fig. 6(*a*). Again, the disappearance of most Bragg and Laue secondary peaks is clearly seen, in contrast to the survival of the surface peaks. The corresponding simulated RS depicted in Fig. 6(*b*) takes into account this surface effect through the diffracted-beam path length. The parameters in the calculation are $a = 5.6534$, $c = 5.6676$ Å, $B_{InGaAs} = 0.60$ Å^2, $\Delta\varphi = 0.045°$ and $\eta = 0.057°$ (1.0×10^{-3} rad). The peak positions in both scans are in very good agreement, as expected; this agreement includes even the $5\bar{5}1$ secondary peak, which is very sensitive to the lattice-parameter change, since its corresponding reciprocal-lattice point is almost tangent to the Ewald sphere. In fact, the angle β between the entry and exit

points from the Ewald sphere is small (11.0954°) for this surface secondary reflection. The small difference in the intensity ratio $111/\bar{1}\bar{3}1$ in both RS is due to the mosaic-spread value used for the calculations: the bigger mosaic spread, the smaller the maximum intensity.

We would like to thank our collegues, M. M. G. de Carvalho at IFGW-UNICAMP and M. A. Sacilotti at CPqD-TELEBRÁS, for the samples used in this study. Thanks are also due to J. M. Sasaki and S. L. Morelhão for valuable suggestions, G. G. Kleiman for revising the manuscript and S. L. Gomes for technical help. Financial support from the Brazilian Institutions CNPq and FAPESP are acknowledged.

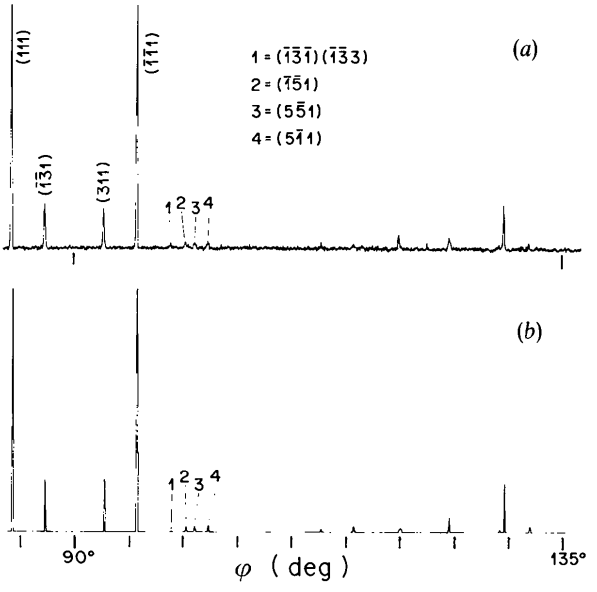

Fig. 6. 002 Renninger scan using Cu $K\alpha_1$ applied to the $In_xGa_{1-x}As$ ternary layer with $x = 0.035$: (*a*) experimental and (*b*) simulated.

References

Barreto, C. L., Carvalho, M. M. G., Ito, K. M. & Fraas, L. M. (1987). *Rev. Fis. Apl. Instrum.* **2**, 307–343.

Caticha-Ellis, S. (1969). *Acta Cryst.* A**25**, 666–673.

Chang, S. L. (1984). *Multiple Diffraction of X-rays in Crystals.* Berlin, Heidelberg, New York, Tokyo: Springer Verlag.

Isherwood, B. J., Brown, B. R. & Halliwell, M. A. G. (1981). *J. Cryst. Growth*, **54**, 449–460.

Lum, R. M., Klingert, J. K., Bylsma, R. B., Glass, A. M., Macrander, A. T., Harris, T. D. & Lamont, M. G. (1988). *J. Appl. Phys.* **64**, 6727–6732.

Morelhão, S. L. & Cardoso, L. P. (1991). *J. Cryst. Growth*, **110**, 543–552.

Morelhão, S. L., Cardoso, L. P., Sasaki, J. M. & Carvalho, M. M. G. (1991). *J. Appl. Phys.* **70**, 2589–2593.

Parente, C. B. R. & Caticha-Ellis, S. (1974). *Jpn. J. Appl. Phys.* **13**, 1501–1505.

Rossmanith, E. (1986). *Acta Cryst.* A**42**, 344–348.

Rossmanith, E., Kumpat, G. & Schulz, A. (1989). *J. Appl. Cryst.* **23**, 99–104.

Sacilotti, M. A. & Bordeaux Rego, A. C. (1989). *Rev. Fis. Apl. Instrum.* **4**, 189–221.

Salles da Costa, C. A. B., Cardoso, L. P., Mazzocchi, V. L. & Parente, C. B. R. (1990). *Defect Control in Semiconductors*, Vol. II, edited by K. Sumino, pp. 1535–1539. Amsterdam: Elsevier.

Soejima, Y., Okazaki, A. & Matsumoto, T. (1985). *Acta Cryst.* A**41**, 128–133.